OPEN ACCESS
IOP Publishing
Superconductor Science and Technology
Supercond. Sci. Technol. **35** (2022) 055005 (5pp)
https://doi.org/10.1088/1361-6668/ac5338

# Laser-lithographically written micron-wide superconducting nanowire single-photon detectors

**Maximilian Protte[1,*], Varun B Verma[2], Jan Philipp Höpker[1], Richard P Mirin[2], Sae Woo Nam[2] and Tim J Bartley[1]**

[1] Mesoscopic Quantum Optics, Department of Physics, Paderborn University, Warburger Str. 100, 33098 Paderborn, Germany
[2] National Institute of Standards and Technology, 325 Broadway, Boulder, CO 80305, United States of America

E-mail: maximilian.protte@upb.de

Received 14 December 2021, revised 25 January 2022
Accepted for publication 9 February 2022
Published 23 March 2022

**Abstract**

We demonstrate the fabrication of micron-wide tungsten silicide superconducting nanowire single-photon detectors on a silicon substrate using laser lithography. We show saturated internal detection efficiencies with wire widths ranging from 0.59 $\mu$m to 1.43 $\mu$m under illumination at 1550 nm. We demonstrate both straight wires, as well as meandered structures. Single-photon sensitivity is shown in devices up to 4 mm in length. Laser-lithographically written devices allow for fast and easy structuring of large areas while maintaining a saturated internal efficiency for wire widths around 1 $\mu$m.

Keywords: superconducting detectors, single-photon detectors, optical lithography, laser lithography

(Some figures may appear in colour only in the online journal)

## 1. Introduction

Superconducting nanowire single-photon detectors (SNSPDs) have had a great impact on modern applied optics experiments, if not revolutionized the field of quantum optics [1]. SNSPDs are used in quantum communication [2], quantum computation [3], as well as light detection and ranging (LIDAR) [4] and deep-space communication [5]. These applications have generally high requirements for the detectors, and detector properties have been highly optimized. Remarkable results including detection efficiencies close to unity [6], extremely low dark counts [7], and timing jitter in the single-picosecond range [8] demonstrate how SNSPDs have outperformed other detector types. Nevertheless, all of these come with the drawback of high requirements for cryogenic temperatures and fabrication tolerances when structuring the superconducting thin films. The latter is especially crucial when investigating complex detector geometries [9], large-scale detectors [10], and multi-element devices [11, 12].

Recent demonstrations of micron-wide superconducting nanowire single-photon detectors with different superconducting materials such as NbN [13–15], MoSi [16–18], and WSi [19, 20] have improved the insight into the fundamental working principle of SNSPDs. In contrast to conventional SNSPD structures, the dimensions of which necessitate e-beam lithography, Chiles *et al* [19] and Lita *et al* [18] were able to use optical mask lithography to structure detectors with

* Author to whom any correspondence should be addressed.



 

saturated internal efficiency, and Wollman *et al* [20] to demonstrate devices with a large active area.

In this paper, we report on our investigations of WSi micron-wide superconducting nanowire single-photon detectors with saturated internal efficiency, structured only with optical laser-lithography for different wire widths. This structuring process enables fast and easy prototyping of arbitrary detector geometries, 'all-in-one-step' structuring of detectors, additional electronics, and contact pads, and fabrication of large-scale devices with reduced stitching of write-fields. In section 2, we present the fabrication process of the WSi-detectors from 400 nm to 1.4 $\mu$m and its fabrication limits. Section 3 contains measurement results of the saturated detection efficiency at 775 nm wavelength as well as 1550 nm wavelength under flood illumination, as well as investigations of dark counts and timing jitter, before concluding in section 4.

## 2. Fabrication

The fabrication process starts with magnetron sputtering of a 2.6 nm thick tungsten silicide film on a silicon substrate as described in [19]. The laser lithography tool for structuring the film uses a wavelength of 375 nm, has a maximum write field of 30 $\mu$m $\times$ 200 mm without stitching and a write speed of 2 mm$^2$ s$^{-1}$. After structuring and subsequent development of the photo resist, the resulting structures are dry etched with $C_4F_8/SF_6$. With this process, we realized SNSPDs in different geometries: straight lines from 100 $\mu$m length to 6 mm length with varying width between 400 nm and 1.4 $\mu$m in 100 nm steps as well as meandered shapes with a wire width of 1 $\mu$m and an unfolded length of 4 mm. For detector geometries of less than 4000 squares, an additional 10 $\mu$m wide 5000 square inductor as well as contact pads were included and written in the same writing step as the SNSPDs. All tested geometries were designed using the PHIDL GDS-layout code [21]. The additional inductor prevents the detectors from latching, due to a sufficiently large kinetic inductance of the device. Figure 1 shows scanning electron microscope (SEM) images of two of the investigated detector designs.

To investigate artifacts in the writing process, the room temperature resistance of 6 mm long stripes with contact pads made out of the same tungsten silicide layer is measured for different wire widths, from 400 nm to 900 nm, as shown in figure 2. While electron-microscope images show a slight increase in sidewall roughness for wire widths at the system specified writing-resolution limit of 400 nm, the measurement data shows the inversely proportional relation of wire width and room-temperature resistance. The sidewall roughness was estimated by taking SEM images of the wire along the detector. Examples can be seen in figures 1(c) and (d).

## 3. Results

For cryogenic investigation of the different detector geometries, several devices were wire-bonded and cooled down in a closed-cycle sorption cryostat with a base temperature of 0.8 K. An SMF-28-Fiber at a distance of 2 mm from the fiber end to the sample surface is used for targeted flood illumination, using an attenuated pulsed lasers of 1550 nm wavelength and 500 kHz repetition rate. Flood illumination refers to the overall illumination of a sample with multiple devices from a single light source, as opposed to fiber coupling individual devices. The attenuation in combination with the light-source distance was chosen such that every detector receives enough photons to discriminate from their dark counts but also not to react to every laser pulse close to their critical current. The setup is shown in figure 3.

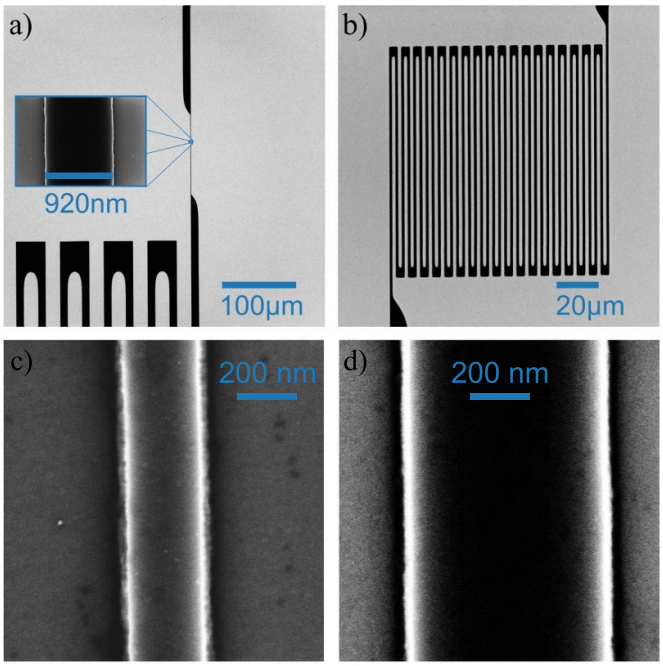


**Figure 1.** SEM image of (a) a 920 nm wide detector wire with serial inductor and (b) a meander design. (c) SEM image of a detector wire with a set width of 400 nm. (d) A 700 nm wide detector wire with smaller sidewall roughness.

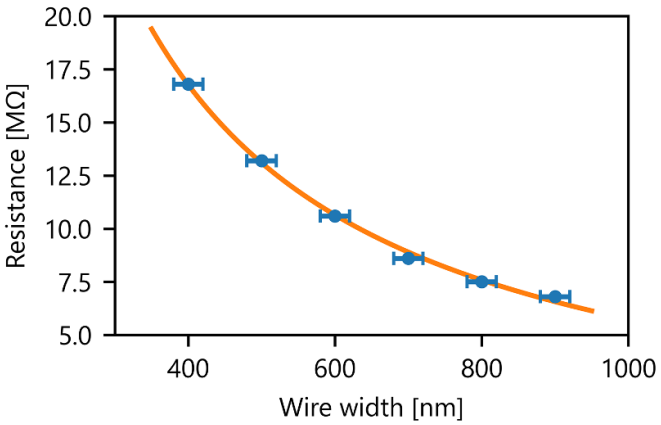


**Figure 2.** Room-temperature resistance of 6 mm long detector wires and contact pads for different wire widths between 400 nm and 900 nm. The inversely proportional relation is illustrated by the fit. The resistance uncertainty arising from the multimeter is too small to be visible and is therefore not included.

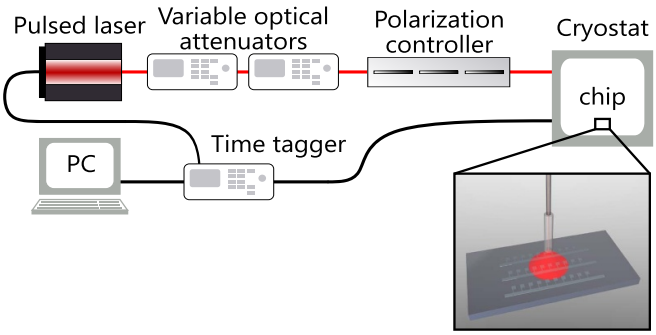


**Figure 3.** Setup used to characterize the detectors. The inset shows schematically the configuration used for flood illumination in the cryostat.

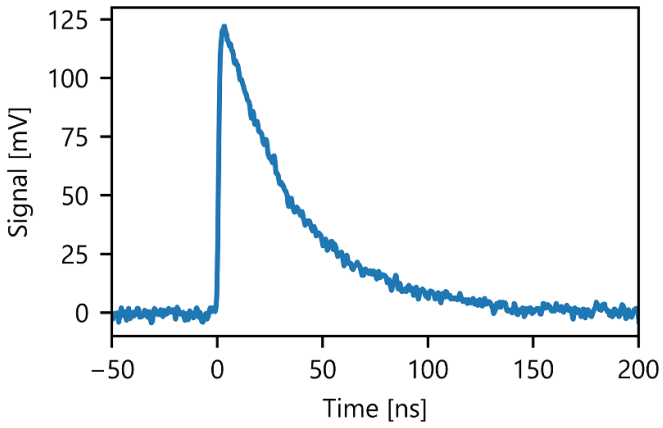


**Figure 4.** Electrical detector response to impinging photons at 1550 nm of a 920 nm wide and 200 $\mu$m long wire with serial inductor at 22 $\mu$A bias current after room-temperature amplification.

Using this setup, the electrical responses to photon absorption of the different detectors are measured. All detectors with widths between 400 nm and 1.4 $\mu$m and lengths between 200 $\mu$m and 6 mm responded to single photons, meaning that when attenuating the laser pulse down to a mean photon number at the single-photon level we are still able to measure detection events. The detector response of a 920 nm wide and 200 $\mu$m long wire with a serial inductor at 22 $\mu$A bias current is shown in figure 4.

A decisive characteristic of SNSPDs is a saturated internal efficiency. This depends on the applied bias current, as only a sufficiently high bias current together with an absorbed photon of certain energy can cause a measurable detection event. For a fixed photon energy there exists a range of bias current, for which the countrate is constant. In this plateau region, the achieved detection efficiency is independent of the bias current which means that the internal detection efficiency is saturated. This can be interpreted as maximizing the probability that when a photon is absorbed a detection event is registered. For the 920 nm wide and 200 $\mu$m long wire with serial inductor, the saturation of the detection efficiency indicated by the plateau

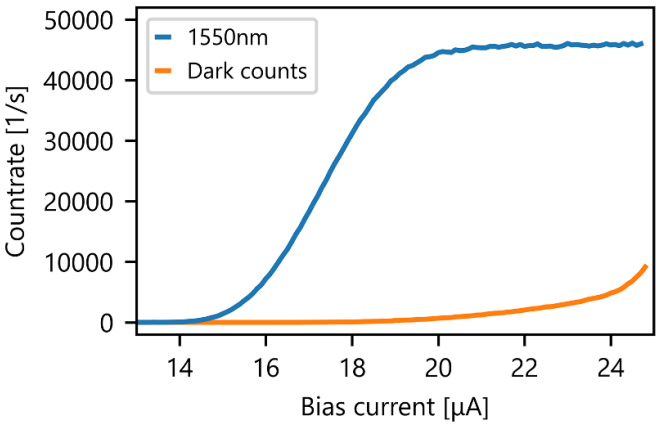


**Figure 5.** Bias-dependent countrate of detection events per second for the 920 nm wide and 200 $\mu$m long wire, measured in coincidence with the arrival time of the laser pulse at 1550 nm wavelength as well as detected dark counts.

of the countrate is shown in figure 5. The statistical errors for the countrates are Poisson noise, for which the error bars are too small in comparison with the data points to be visible. This applies to all displayed countrates. A saturated internal efficiency is important to achieve detector systems with high system efficiencies. We have not taken any actions to optimize the collection and absorption efficiency for high system efficiencies. The reduced countrate compared to the repetition rate of the laser results from the laser's mean photon number together with the non-optimized collection and absorption efficiency of the system, meaning that a detection event does not always occur for each pulse, since no photon is absorbed by a detector. The plateau indicates sufficient fabrication tolerances using laser lithography since reaching a plateau is mainly restricted by the fabrication imperfections for photons in the near-infrared spectral range. As the detector responses were measured in coincidence with the pulsed laser, no additional dark-count subtraction was executed, as the number of dark counts was negligible in a total of 1 ms active measurement time. Therefore, the shown representative dark-count data was taken independently.

Furthermore, the results for similar devices with wire widths from 590 nm to 1430 nm are presented in figure 6. Results for wire widths smaller than 590 nm are not included since they respond to impinging photons but not show a saturated detection efficiency. The absolute countrates of each detector varies due to different collection efficiencies caused by the different active areas as well as the relative fiber position.

In addition, we measured a representative timing jitter of 225 ps for the 920 nm wide detector, as shown in figure 7, using the pulsed laser at 1550 nm wavelength with a pulse width of 9 ps. Jitter contributions from 5 mm long wire bonds, the laser synchronisation, or time tagger were not deconvoluted. A deconvolution would lead to a smaller timing jitter.

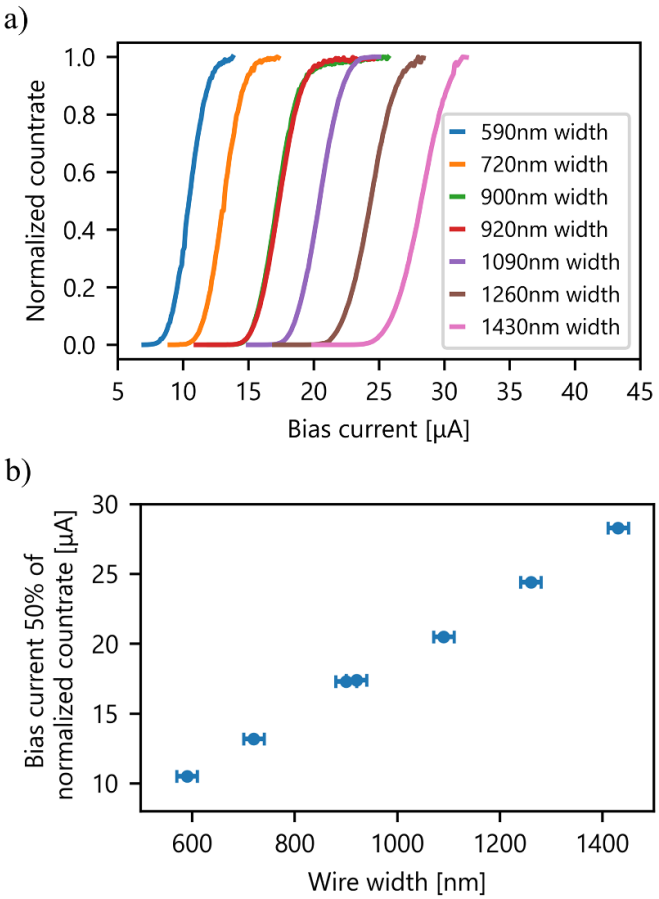


**Figure 6.** (a) Bias-dependent countrate of detection events per second at 1550 nm wavelength for different wire widths, measured in coincidence with the arrival time of the laser pulse and normalized to their maximum countrate before latching. The red graph for a 920 nm wide device corresponds to the measurement data in figure 5 with more detail. (b) Bias current values at 50% of the maximum countrate based on the data from figure (a) for different detector-wire widths. The wire width and displayed error bars are based on SEM width measurements. The error on the bias-current is inferred from the Poisson noise limited countrate, which is negligible.

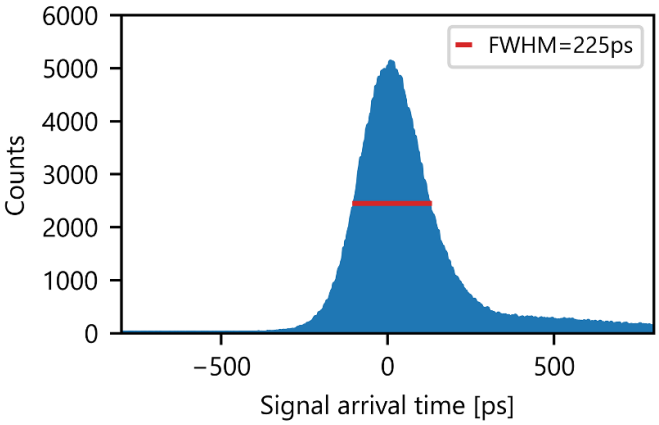


**Figure 7.** Jitter measurement of the 920 nm wide and 200 $\mu$m long tungsten silicide wire with serial inductor for 1550 nm photons, showing a full width at half maximum of 225 ps.

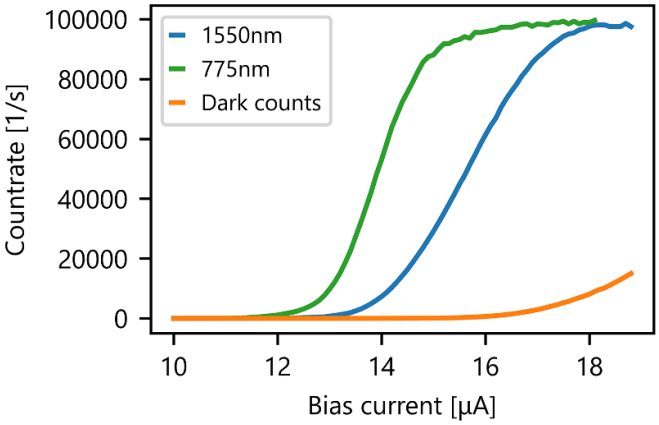


**Figure 8.** Bias-dependent countrate of detection events per second for the 1 nm wide and 4 mm long meander using the pulsed lasers at 1550 nm and 775 nm wavelength, measured in coincidence with the arrival time of the laser pulse as well as detected dark counts.

As imperfections in the fabrication steps are particularly critical for large-area devices, we also investigated the bias-dependence of the detection efficiency for a 1 $\mu$m wide and 4 mm long detector folded into a meander shape, as depicted in figure 1(b) for 1550 nm photons as well as 775 nm photons. This devices also shows a plateau region for both wavelengths, as shown in figure 8. Comparing the range of bias currents at which the countrate saturates, for the meander design and straight lines with comparable wire width, the shorter plateau region of the meander design can most likely be attributed to limitations in the writing accuracy using laser lithography or to inhomogeneities in the thin film.

## 4. Conclusion

In this work, we investigated laser-lithographically written SNSPDs with widths between 400 nm and 1.4 $\mu$m and lengths between 200 $\mu$m and 6 mm. We demonstrated saturated detection efficiency at 775 nm wavelength and 1550 nm wavelength. So far, our results show that increasing the detector length can result in a shorter plateau length, due to an increased chance of fabrication imperfections. The realization of laser-lithographically written SNSPDs enables easy and fast prototyping as well as structuring of large-scale SNSPD arrays, which we want to extend in the future. In addition, micron-wide detectors can be used to drastically enhance the efficiency of integrated SNSPDs on low-index-contrast

waveguides as UV-written waveguides in silica or titanium in-diffused wafeguides in lithium niobate.

## Acknowledgment

The study was partially funded by Bundesministerium für Bildung und Forschung (13N14911).

## ORCID iDs

Maximilian Protte https://orcid.org/0000-0001-6672-4771
Jan Philipp Höpker https://orcid.org/0000-0002-8174-0734

## References

[1] You L 2020 Superconducting nanowire single-photon detectors for quantum information *Nanophotonics* **9** 2673–92
[2] Yin J *et al* 2017 Satellite-based entanglement distribution over 1200 kilometers *Science* **356** 1140–4
[3] Zhong H-S *et al* 2020 Quantum computational advantage using photons *Science* **370** 1460–3
[4] Taylor G G, Morozov D, Gemmell N R, Erotokritou K, Miki S, Terai H and Hadfield R H 2019 Photon counting LIDAR at 2.3$\mu$m wavelength with superconducting nanowires *Opt. Express* **27** 38147–58
[5] Grein M E, Kerman A J, Dauler E A, Willis M M, Romkey B, Molnar R J, Robinson B S, Murphy D V and Boroson D M 2015 An optical receiver for the lunar laser communication demonstration based on photon-counting superconducting nanowires *Proc. SPIE* **9492** 949208
[6] Reddy D V, Nerem R R, Nam S W, Mirin R P and Verma V B 2020 Superconducting nanowire single-photon detectors with 98% system detection efficiency at 1550 nm *Optica* **7** 1649–53
[7] Hochberg Y, Charaev I, Nam S W, Verma V B, Colangelo M and Berggren K K 2019 Detecting sub-GeV dark matter with superconducting nanowires *Phys. Rev. Lett.* **123** 151802
[8] Korzh B *et al* 2020 Demonstration of sub-3 ps temporal resolution with a superconducting nanowire single-photon detector *Nat. Photon.* **14** 250–5
[9] Meng Y, Zou K, Hu N, Lan X, Xu L, Zichi J, Steinhauer S, Zwiller V and Hu X 2020 Fractal superconducting nanowire avalanche photodetector at 1550nm with 60% system detection efficiency and 1.05 polarization sensitivity *Opt. Lett.* **45** 471–4
[10] Steinhauer S, Gyger S and Zwiller V 2021 Progress on large-scale superconducting nanowire single-photon detectors *Appl. Phys. Lett.* **118** 100501
[11] Allman M S *et al* 2015 A near-infrared 64-pixel superconducting nanowire single photon detector array with integrated multiplexed readout *Appl. Phys. Lett.* **106** 192601
[12] Wollman E E, Verma V B, Lita A E, Farr W H, Shaw M D, Mirin R P and Nam S W 2019 Kilopixel array of superconducting nanowire single-photon detectors *Opt. Express* **27** 35279–89
[13] Korneeva Y P, Vodolazov D Y, Semenov A V, Florya I N, Simonov N, Baeva E, Korneev A A, Goltsman G N and Klapwihk T M 2018 Optical single-photon detection in micrometer-scale NbN bridges *Phys. Rev. Appl.* **9** 064037
[14] Vodolazov D Y, Manova N N, Korneeva Y P and Korneev A A 2020 Timing jitter in NbN superconducting microstrip single-photon detector *Phys. Rev. Appl.* **14** 044041
[15] Guang-Zhao X *et al* 2020 Superconducting microstrip single-photon detector with system detection efficiency over 90% at 1550 nm *Photon. Res.* **9** 958–67
[16] Charaev I, Morimoto Y, Dane A, Agarwal A, Colangelo M and Berggren K K 2020 Large-area microwire MoSi single-photon detectors at 1550 nm wavelength *Appl. Phys. Lett.* **116** 242603
[17] Korneeva Y P, Vodolazov D Y, Semenov A V, Florya I N, Simonov N, Baeva E, Korneev A A, Goltsman G N and Klapwihk T M 2020 Different single-photon response of wide and narrow superconducting $Mo_xSi_{1-x}$ strips *Phys. Rev. Appl.* **13** 024011
[18] Lita A E, Verma V B, Chiles J, Mirin R P and Nam S W 2021 $Mo_xSi_{1-x}$ a versatile material for nanowire to microwire single-photon detectors from UV to near IR *Supercond. Sci. Technol.* **34** 054001
[19] Chiles J *et al* 2020 Superconducting microwire detectors based on WSi with single-photon sensitivity in the near-infrared *Appl. Phys. Lett.* **116** 242602
[20] Wollman E E *et al* 2019 Recent advances in superconducting nanowire single-photon detector technology for exoplanet transit spectroscopy in the mid-infrared *J. Astron. Telesc. Instrum. Syst.* **7** 011004
[21] McCaughan A N, Taits A M, Buckley S M, Oh D M, Chiles J T, Shainline J M and Nam S W 2021 PHIDL: Python CAD layout and geometry creation for nanolithography (arXiv:2103.01152)